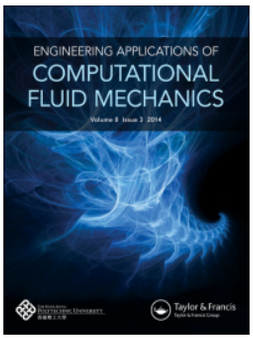

Taylor & Francis
Taylor & Francis Group

Engineering Applications of Computational Fluid Mechanics

ISSN: (Print) (Online) Journal homepage: https://www.tandfonline.com/loi/tcfm20

Numerical investigation of magnetic field on forced convection heat transfer and entropy generation in a microchannel with trapezoidal ribs

Lixuesong Han, Chenji Lu, Alexei Yumashev, Dariush Bahrami, Rasool Kalbasi, Mehdi Jahangiri, Arash Karimipour, Shahab S. Band, Kwok-Wing Chau & Amir Mosavi

To cite this article: Lixuesong Han, Chenji Lu, Alexei Yumashev, Dariush Bahrami, Rasool Kalbasi, Mehdi Jahangiri, Arash Karimipour, Shahab S. Band, Kwok-Wing Chau & Amir Mosavi (2021) Numerical investigation of magnetic field on forced convection heat transfer and entropy generation in a microchannel with trapezoidal ribs, Engineering Applications of Computational Fluid Mechanics, 15:1, 1746-1760, DOI: 10.1080/19942060.2021.1984991

To link to this article: https://doi.org/10.1080/19942060.2021.1984991

Published online: 29 Oct 2021.

ENGINEERING APPLICATIONS OF COMPUTATIONAL FLUID MECHANICS
2021, VOL. 15, NO. 1, 1746–1760
https://doi.org/10.1080/19942060.2021.1984991

Taylor & Francis
Taylor & Francis Group

Numerical investigation of magnetic field on forced convection heat transfer and entropy generation in a microchannel with trapezoidal ribs

Lixuesong Han[a], Chenji Lu[b], Alexei Yumashev[c], Dariush Bahrami [d], Rasool Kalbasi[e], Mehdi Jahangiri[f], Arash Karimipour[e], Shahab S. Band[g], Kwok-Wing Chau [h] and Amir Mosavi [i,j,k]

[a]School of Physical Science and Technology, ShanghaiTech University, Shanghai, People's Republic of China; [b]Department of Aeronautical and Astronautical Engineering, University of Southampton, Southampton, UK; [c]Department of Prosthetic Dentistry, The State Education Institution of Higher Professional Training, The First Sechenov Moscow State Medical University under Ministry of Health of the Russian Federation, Moscow, Russian Federation; [d]Department of Mechanical Engineering, Shahrekord University, Shahrekord, Iran; [e]Department of Mechanical Engineering, Najafabad Branch, Islamic Azad University, Najafabad, Iran; [f]Department of Mechanical Engineering, Shahrekord Branch, Islamic Azad University, Shahrekord, Iran; [g]Future Technology Research Center, College of Future, National Yunlin University of Science and Technology, Douliou, Taiwan; [h]Department of Civil and Environmental Engineering, Hong Kong Polytechnic University, Hong Kong, People's Republic of China; [i]Faculty of Civil Engineering, Technische Universität Dresden, Dresden, Germany; [j]John von Neumann Faculty of Informatics, Obuda University, Budapest, Hungary; [k]Department of Informatics, J. Selye University, Komarno, Slovakia

ABSTRACT

In this study, the effects of adding trapezoidal ribs to microchannel on functionalized multi-walled nano-tubes/water nanofluid heat transfer are examined. The dimensionless slip coefficient (0–0.1), Reynolds number (50–400) and Hartmann number (0–20) are considered as independent variables and the heat transfer along with the entropy generation are considered as the output parameters. The simulation outcomes confirm that the addition of trapezoidal ribs, on the one hand, increases the heat transfer area and, on the other hand, intensifies the possibility of vortex formation. The presence of a vortex decreases the heat transfer potential and thus reduces the performance of the trapezoidal-wall microchannel compared to the base one. With increasing Reynolds number (Re), the probability of vortex formation intensifies, which in turn diminishes the positive effects of using trapezoidal ribs. However, it is found that, with increasing Hartmann number (Ha) and dimensionless slip coefficient (β^*), the vortex strength is weakened, and consequently heat transfer is improved. Based on numerical computations, it is found that at Re = 400, Ha = 0 and $\beta^* = 0$ and adding trapezoidal ribs to the base microchannel increases heat transfer by 11.12%.

ARTICLE HISTORY
Received 8 September 2020
Accepted 20 September 2021

KEYWORDS
Trapezoidal ribs; vortex; entropy generation; magnetic field; nanofluid; slip

1. Introduction

Looking at the history of applicable devices, it can be seen that advances in technology have always changed the size of objects (Dinarvand et al., 2017; Sheikholeslami and Rokni, 2017). This resizing has often led to size reduction on mille, micro and even nanoscales. Size reduction in equipment such as electronic devices (Kalbasi, 2021; Muhammad et al., 2020), pumps (Alipour et al., 2019), turbines (Xu et al., 2019) and microfluidics (Bayareh, 2020), are examples of resizing. Size reduction in the flow area leads to microchannels, which provide more heat transfer area per unit volume than conventional ducts (Abdollahi et al., 2020; Bayareh et al., 2020). Thermal and hydraulic behavior in microchannels can be improved by various techniques such as the use of nanofluids (Arjmandfard et al., 2020; K. G. Dehkordi, Karimipour, et al., 2021; Turkyilmazoglu, 2016, 2020b, 2020c, 2021), magnetic fields (MFs) (R. B. Dehkordi, Toghraie, et al., 2021; Dinarvand et al., 2021; Turkyilmazoglu, 2011; Turkyilmazoglu, 2020a; Zhong et al., 2021) and installing ribs (Akermann et al., 2020; Jiang et al., 2020).

Alfellag et al. (2020) examined the effects of installing inclined plate-fins on the hydrothermal performance of a minichannel. Numerical results showed that the Nusselt number (Nu) increased with increasing slotted height up to 1.5. Additionally, their minichannel hydrothermal efficiency and heat transfer are about 1.84 and 1.54 times more than those of a simple one.

CONTACT Amir Mosavi amir.mosavi@mailbox.tu-dresden.de; Shahab S. Band shamshirbands@yuntech.edu.tw

The effects of installing triangular ribs on the walls of a microchannel in which an MF has been exerted were investigated by Nguyen, Bahrami, Kalbasi, and Bach (2020). Internal extended surfaces (ribs) can have two simultaneous effects: on the one hand, they increased heat exchange by increasing the heat transfer area, and on the other hand, a vortex could form behind each rib, which drastically diminishes heat transfer. The presence of an MF weakens the vortex and thus improved heat transfer. Eventually through adding extended surfaces as well as MFs, heat transfer and entropy generation are intensified by 25% and 328%, respectively.

The effect of installing different ribs in a U-shaped channel was numerically simulated by Ravi et al. (2017). They focused on heat transfer and found that the presence of ribs in the channel increases heat transfer. They proved that heat transfer can be enhanced up to 35% by using V-shaped ribs.

Table 1 summarizes the results of studies that were focused on heat transfer improvement using ribs. In another work, Bahrami, Nadooshan, et al. (2020) applied an MF to mix magnetic particles in water numerically. Their result strongly confirmed that there is an optimum value in the strength of an MF to produce a high mixing performance. Nojoomizadeh and Karimipour (2016) investigated heat transfer within a microchannel in the presence of multi-walled cabon nano-tubes (MWCNT)/oil nanofluid applying a slip condition. Their microchannels were considered porous and the results showed that changing the Darcy number as well as the nanofluid volume fraction could lead to an improvement in the amount of heat exchange.

Karimipour et al. (2017), by using computational fluid dynamics techniques, examined a microchannel (with slip condition) in the presence of an MF and revealed that that the MF exerted a resistive force. By comparing two kinds of nanoparticle (Ag and Al_2O_3), they found that Ag nanoparticles performed 20% better than Al_2O_3 in heat transfer.

Forghani-Tehrani et al. (2017) studied a microchannel containing silver/water nanofluid under variable heat flux. In their work, they considered the microchannel in two scenarios. In the first scenario, a slip condition was applied, while in the second one, zero velocity was considered for the wall. They proved that, when the slip coefficient increased, the slip velocity along the wall also grew and an MF could amplify this velocity.

The effects of exerting an MF on heat exchange between a functionalized multi-walled carbon nanotubes (FMWCNT)/water nanofluid and the wall of a microchannel with triangular ribs were investigated by Shiriny et al. (2019). They applied a slip condition and affirmed that the slip velocity along the wall did not always amplify heat transfer. They reported that, at high volume fraction, an MF boosted heat transfer by 20%.

Mohebbi et al. (2018) used the lattice Boltzmann approach to evaluate nanofluid flow heat transfer from a microchannel equipped with square ribs. They found that applying nanofluid had positive effects on heat transfer. They revealed that increasing nanofluid volume fraction from 0 to 0.05 caused an approximately 40% improvement in heat transfer.

Karimipour et al. (2020) simulated a microchannel equipped with injections by exerting an MF. They proved

Table 1. A summary of studies using different ribs.

Authors	Problem	Effect of	Result
Gravndyan et al. (2017)	Microchannel	Rib aspect ratios (AR = 10, 15, 20, 25)	The rib with AR = 10 and AR = 25 led to the highest and lowest PEC. The increment of the rib pitch at higher fluid velocity led to more pressure drop.
Wang et al. (2019)	Microchannel	Bidirectional rib	Up to 200% increase in the pressure drop.
Shen et al. (2017)	Microchannel	Y-shaped metal foams attached with rib	44% decrement in thermal resistances.
Wang et al. (2015)	Microchannel	Micro-scale ribs	Heat transfer in microchannel with ribs was 1.11 ~ 1.55 times better than that in the smooth one.
Bahrami et al. (2020)	Microchannel	Injectable rib	46.4% boosting in the heat transfer. 234% drop in entropy generation.
Salman (2019)	Tube	Comparing triangular, rectangular and trapezoidal ribs	Maximum heat transfer corresponded to the triangular rib. Up to 44% enhancement in heat transfer observed compared smooth microchannel.

that the presence of nanofluid, as well as an MF, greatly improved forced convection heat transfer.

Cheng et al. (2021) proposed a wavy microchannel to make vortices in order to boost heat transfer. Their microchannel included several heat sources. They revealed that the rate of heat transfer improves as the inlet velocity increases as a result of higher and stronger vortices. However, in a smooth microchannel the heat transfer was lower due to the lack of vortices.

Samadifar and Toghraie (2018) applied a wide range of vortex generators to improve the efficiency of a heat exchanger. Their observations confirmed that vortex generation with a rectangle shape is much more effective than other forms of geometry.

Bahrami, Abbasian-Naghneh, et al. (2020) proposed a microchannel with a slip condition and ribs. In their work, nanofluid moved through the ribs, which resulted in vortices being generated. They found that the rib height affected heat transfer by creating vortices and irreversibility, and as the inlet velocity increased the vortices became stronger. Based on these results, the former and latter were amplified by 46.4% and 45.3%, respectively, owing to the increase in rib height.

Gallegos and Sharma (2017) used a flexible plate to make a vortex in order to increase convective heat transfer. They proved that, when the plate is rigid, there is no vortex, whereas a flexible plate creates a considerable number of vortices, which increases the thermal efficiency.

In another study, Nguyen, Bahrami, Kalbasi, and Karimipour (2020) changed an inner smooth wall of a double-pipe heat exchanger to a sinusoidal-wall to increase the heat transfer area. They found that the vortex formation in the diverging section did not allow heat transfer to improve. At best, the heat exchanger effectiveness was improved by 1.56%. To reduce the strength of vortices, they exerted an MF and showed that the effectiveness could be improved by 19%. The sinusoidal walls generated a vortex and thus increased irreversibility by 18%, which could be reduced from 18% to 8% by applying an MF.

A literature review revealed that the efficacy of adding trapezoidal ribs on improving heat transfer, as well as entropy generation, had not been investigated. The presence of trapezoidal ribs seems to have two effects. On the one hand, they increase the heat transfer area and therefore have a positive effect on heat exchange between FMWNT/water nanofluid flow and microchannel walls. On the other hand, they might cause vortex formation that negatively affects heat exchange. In this study, an MF is applied to diminish the negative effects of the vortex. However, the MF intensifies the resistive forces and thus amplifies the pressure drop. In this way, by computing the entropy generation, the behavior of a simple microchannel can be compared with the modified microchannel (equipped with trapezoidal ribs and under the influence of an MF) from the second law perspective.

2. Problem description

Figure 1 shows a microchannel with trapezoidal ribs as internal extended surfaces. The microchannel height is 100 μm and the ratio of the length to the height is considered to be 40.

Considering $a = 120\,\mu m$ and $b = 360\,\mu m$, the geometric characteristics of the trapezoidal ribs can be specified. The nanofluid of the FMWNT/water enters the microchannel at $T_c = 293\,K$ and leaves the microchannel after exchanging heat with the trapezoidal ribs at $T_h = 300\,K$. The nanofluid flow is considered to be laminar with a Reynolds number (Re) of 50–400. As shown in Figure 1, a magnetic field MF (at Hartmann numbers Ha up to 20) is exerted. A slip boundary condition is applied on the walls and the results are compared with the non-slip condition. Table 2 presents the thermo-physical properties of FMWNT/water.

3. Mathematical formulation

The main purpose of this study is to compute the rate of heat exchange between nanofluid flow and microchannel walls, which depends on the temperature gradient. The temperature gradient in the solution domain is obtained by solving the energy equation (Afrand et al., 2016):

$$u\frac{\partial T}{\partial x} + v\frac{\partial T}{\partial y} = \alpha_{nf}\left(\frac{\partial^2 T}{\partial x^2} + \frac{\partial^2 T}{\partial y^2}\right) \tag{1}$$

In the above equation, u and v are the velocity in the x- and y-directions, respectively, T is temperature and $\alpha_{nf} = k_{nf}/\rho_{nf}C_{nf}$ denotes the thermal diffusivity. Moreover, k_{nf}, ρ_{nf} and c_{nf} are the thermal conductivity, density, and heat capacity of the nanofluid, respectively. The property values are reported in Table 2. The velocity components are determined through solving the momentum/continuity equations in the horizontal (x) and vertical (y) directions:

$$\frac{\partial u}{\partial x} + \frac{\partial v}{\partial y} = 0 \tag{2}$$

$$u\frac{\partial u}{\partial x} + v\frac{\partial u}{\partial y} = -\frac{1}{\rho_{nf}}\frac{\partial p}{\partial x} + \frac{\mu_{nf}}{\rho_{nf}}\left(\frac{\partial^2 u}{\partial x^2} + \frac{\partial^2 u}{\partial y^2}\right) - \frac{\sigma_{nf}B_0^2}{\rho_{nf}}u \tag{3}$$

$$v\frac{\partial v}{\partial x} + v\frac{\partial v}{\partial y} = -\frac{1}{\rho_{nf}}\frac{\partial p}{\partial y} + \frac{\mu_{nf}}{\rho_{nf}}\left(\frac{\partial^2 v}{\partial x^2} + \frac{\partial^2 v}{\partial y^2}\right) \tag{4}$$

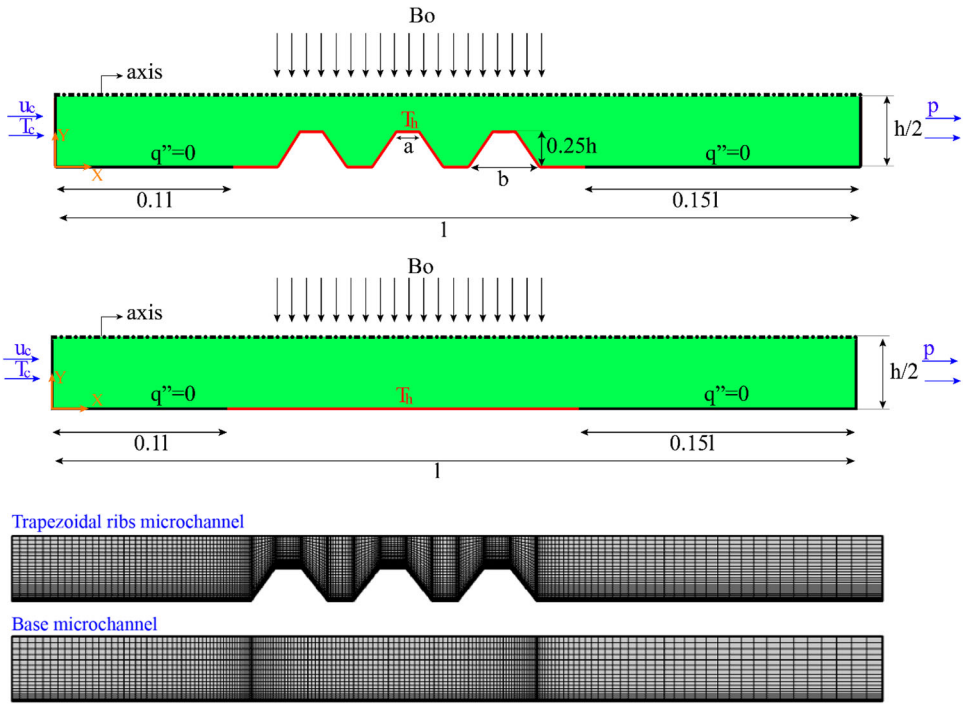

Figure 1. The 'base' microchannel and microchannel with trapezoidal ribs.

Table 2. FMWNT nanofluid properties (Amrollahi et al., 2010).

ϕ (%)	ρ_{nf}(kg/m^3)	k_{nf}(W/m · K)	μ_{nf} (Pa · s)
0	995.8	0.59	9.8×10^{-4}
0.12%	1003	0.65	9.98×10^{-4}

where μ_{nf} is the viscosity of the nanofluid and p is the pressure. Note that the term $\left(\frac{\sigma_{\mathrm{nf}} B_0^2}{\rho_{\mathrm{nf}}} u\right)$ denotes the resistive force exerted by the magnetic field (the Lorentz force). Additionally, B_0 and σ_{nf} are the magnetic intensity and nanofluid electrical conductivity, respectively (Afrand et al., 2016). It should be noted that nanofluid flow is considered under steady, incompressible, laminar and single phase. The boundary conditions are as follows:

$$u = u_c,\ v = 0,\ T = T_c \quad \text{inlet} \quad (x = 0,\ 0 \le y \le h) \tag{5}$$

$$\frac{\partial u}{\partial x} = 0,\ v = 0,\ \frac{\partial T}{\partial x} = 0 \quad \text{outlet} \quad (x = l,\ 0 \le y \le h) \tag{6}$$

$$\begin{aligned} &\text{velocity along the lower wall} = u_s, \qquad \text{at lower wall} \\ &\text{velocity normal to the lower wall} = 0, \end{aligned} \tag{7}$$

$$\begin{aligned} &T = 0.1T_h \quad 1 \le x \le 0.75\,l \quad \text{for upper wall} \\ &u = u_s \quad , \quad v = 0 \qquad\qquad \text{at upper wall} \\ &T = 0.1T_h \quad 1 \le x \le 0.75\,l \quad \text{for upper wall} \end{aligned} \tag{8}$$

where u_c and T_c are the nanofluid's incoming velocity and temperature, respectively. Additionally, u_s denotes the slip velocity and is obtained by the following equation:

$$\begin{aligned} u_s &= \pm\beta\left(\frac{\partial u}{\partial n}\right)_{\substack{\text{at upper and} \\ \text{lower walls}}} \\ \mu\frac{\partial u}{\partial n} &= \tau \end{aligned} \tag{9}$$

where β is the slip coefficient.

In present work, the authors consider some separated linear parts along the bottom boundary. This means that the slip velocity is simulated along all these linear boundaries step by step; and finally all of them would be just plotted continuously in the one figure. The positive and negative coefficients correspond to the lower and upper walls of the microchannel, respectively. In this study, the results are presented in terms of dimensionless numbers according to the following equations:

$$\begin{aligned} &\beta^* = \frac{\beta}{h},\ U_s = \pm\beta^*\frac{h^2}{u_c}\left(\frac{\partial u}{\partial n}\right)_{\text{at upper and lower walls}}, \\ &\theta = \frac{T - T_c}{T_h - T_c}, \mathrm{Re} = \frac{u_c h}{\vartheta_{nf}}, \\ &Ha = B_0 h\left(\frac{\sigma_{nf}}{\mu_{nf}}\right)^{0.5} \end{aligned} \tag{10}$$

In the above dimensionless equations, β^*, U_s and θ are slip coefficient, slip velocity and dimensionless temperature, respectively.

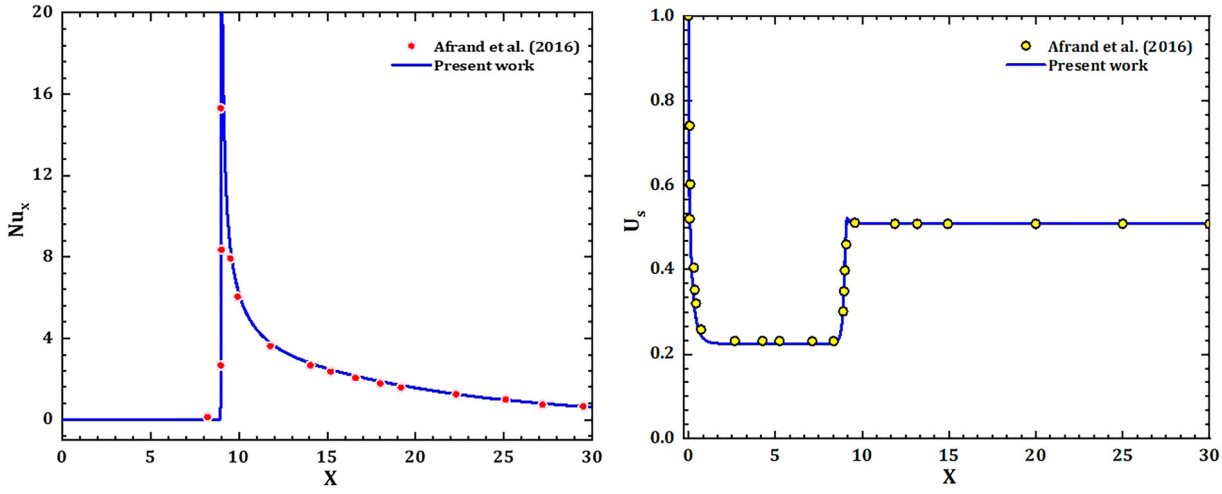

Figure 2. Validation of the solution method.

The local and average Nusselt numbers are obtained by the following equations (Nguyen, Bahrami, Kalbasi, & Bach, 2020):

$$Nu_x = -\frac{k_{nf}h}{k_f}\left(\frac{\partial\theta}{\partial y}\right)_{y=0,h}$$
$$Nu_{ave} = \frac{1}{l}\int_0^l Nu_x\,dx \tag{11}$$

The computations correspond to the study of the second law leading to entropy generation, which includes viscous and thermal terms and is obtained from the following equations (Nguyen, Bahrami, Kalbasi, & Bach, 2020):

$$\dot{s}_{th} = \iint \frac{k_{nf}}{T^2}\left[\left[\left(\frac{\partial T}{\partial x}\right)^2 + \left(\frac{\partial T}{\partial y}\right)^2\right]\right] dA \tag{12}$$

$$\dot{s}_f = \iint \left(\frac{\mu_{nf}}{T}\left[2\left[\left(\frac{\partial u}{\partial x}\right)^2 + \left(\frac{\partial v}{\partial y}\right)^2\right] + \left(\frac{\partial u}{\partial y} + \frac{\partial v}{\partial x}\right)^2\right] + \frac{\sigma_{nf}(v/u_c)^2 B_0^2}{T}\right) dA \tag{13}$$

where $\dot{s}_{th}$ and $\dot{s}_f$ are the thermal and viscous terms, respectively.

4. Validation and grid study

All governing equations and boundary conditions are solved by the finite volume method. For the discretization of the balance equations, a second-order scheme is used. For coupling velocity and pressure, the SIMPLE algorithm is implemented. Additionally, double precision convergence criteria of 10^{-6} and 10^{-16} are applied for fluid and energy equations, respectively. For validity, the present numerical study is compared with that of Afrand et al. (2016). They considered a smooth microchannel at $\beta^* = 0.05$ and $Re = 20$, and exerted Lorentz force through applying magnetic field ($Ha = 20$). Numerical results for Nu_x as well as U_s along the microchannel for the study conducted by Afrand et al. (2016) are presented in Figure 2 and compared with the present simulations. There is good agreement between the results and it can be claimed that the method of solving the balance equations in this study can well simulate the hydrothermal behavior of microchannels.

The main purpose of this paper is to investigate heat transfer from the microchannel. A schematic of the mesh is illustrated in Figure 1. To examine the mesh independency, Nusselt number variations at 0.125 vol.%, $Re = 100$ and $Ha = 20$ are inspected. Figure 3 presents the values of Nu_{ave} with respect to the number of computational cells and it is found that a network with 11,600 nodes is appropriate.

5. Results and discussion

Heat transfer, pressure drop and entropy generation depend on the temperature and velocity gradients so that larger gradients will lead to higher values of these parameters. The results are presented within the ranges $50 \le Re \le 400$, $0 \le Ha \le 20$ and $0 \le \beta^* \le 0.1$. In the following, the streamlines and isotherms in the microchannel are illustrated to identify regions with high velocity and temperature gradients.

5.1. Streamlines and isotherms

Figure 4 illustrates the streamlines and isotherms at $Re = 400$ at $0 \le \beta^* \le 0.1$. Because the bottom wall of the microchannel is of trapezoidal shape, flow separation

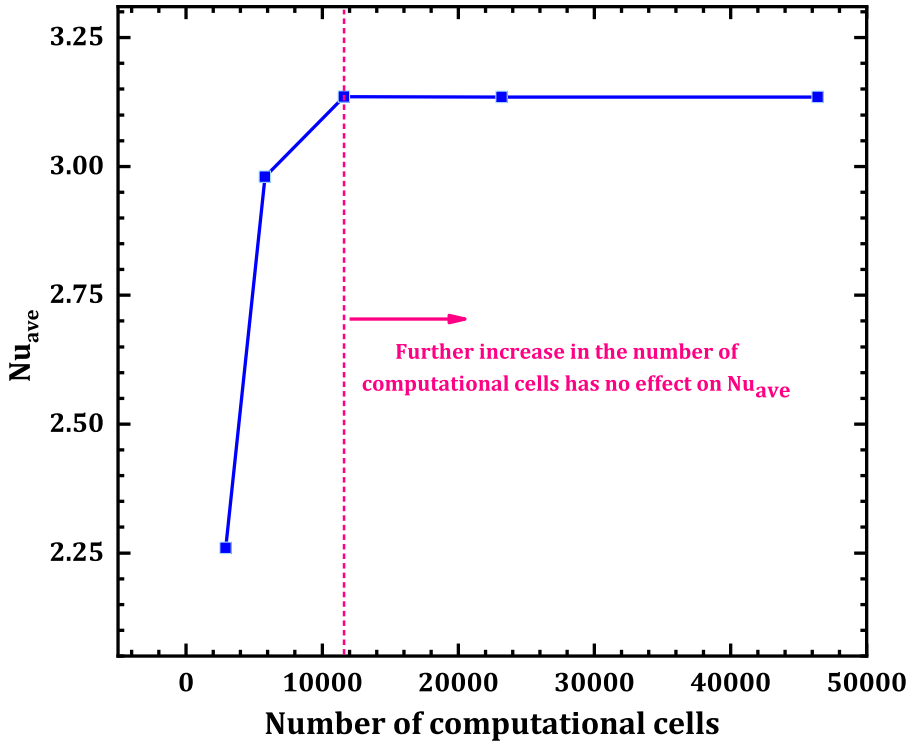

Figure 3. Grid study.

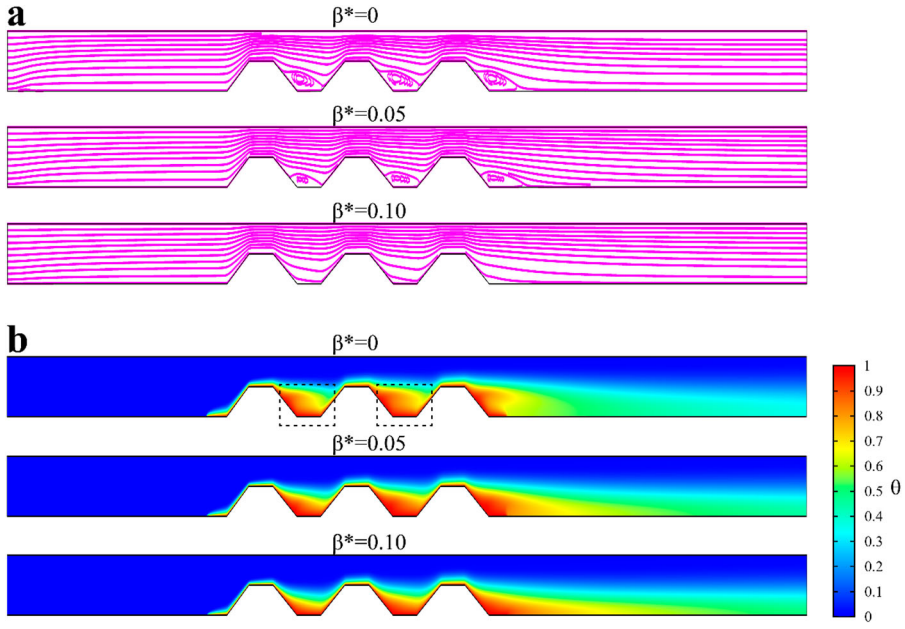

Figure 4. Streamlines and isotherms at various β^* (Re = 400 and Ha = 5).

is expected to occur in the divergent part of the trapezoid, which consequently creates a vortex. Figures 4 and 5 show that trapezoidal ribs create a vortex. In this study, the effect of two parameters, namely β^* and Ha, on the strength of a vortex is investigated. The main purpose of installing trapezoidal ribs is to boost the heat transfer area, which in turn intensifies the needed heat transfer. But unfortunately, these types of rib produce vortices and therefore affect and reduce the ribs' efficacy. One way to diminish the strength of a vortex is to apply slip velocities (as shown in Figure 4).

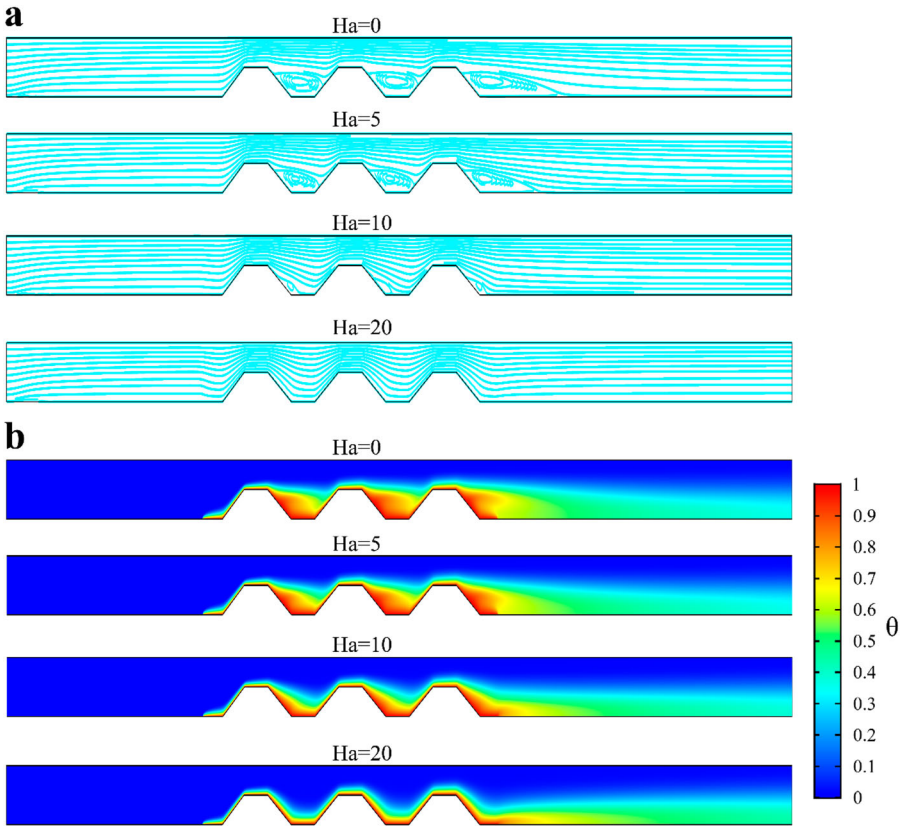

Figure 5. Streamlines and isotherms at various Ha (Re = 400 and $\beta^* = 0$).

In the case where β^* is zero (non-slip), several vortices are observed in Figure 4. As β^* rises to 0.05, the zone under the effects of the vortex (the zone affected by the vortex) becomes smaller. With a further increase in β^* (from 0.05 to 0.1), it is observed that the vortex has become so weak that the zone affected by the vortex is not easily discernible.

On the other hand, the effect of the slip coefficient on isotherms is also significant. It is observed that, with increasing β^*, the temperature distribution is limited to the regions next to the wall and hence the temperature gradient increases.

Applying a magnetic field is another technique for diminishing vortex intensity. Streamlines and isotherms are also sensitive to the presence of a magnetic field. Figure 5 shows streamlines as well as isotherms at different Hartmann numbers.

As shown in Figure 5, the trapezoidal wall separates the flow and creates vortices. It is clear that, as Ha rises, the vortices become weaker or the zone affected by vortices is reduced. Hence, the isotherm density close to the wall amplifies, which means that heat transfer is enhanced by Ha growth. Finally, it can be claimed that, with increasing Ha and slip coefficient, the vortex strength is weakened and consequently heat transfer is improved.

5.2. Nusselt number

Figure 6 shows the variations in Nu_x along the walls of the base and trapezoidal-wall microchannels, respectively, at Re = 200 and $\beta^* = 0.05$.

For the base microchannel, it can be seen that Nu_x decreases at Ha = 0 as well as at Ha = 20. This is because the thickness of the boundary layer starts to grow from the beginning of the microchannel and increases along the microchannel. Consequently, temperature gradients decrease, and hence Nu_x is reduced. A remarkable point is a higher Nu_x at a higher Hartmann number (Ha = 20). It is because the MF exerts a resistive force (Lorentz force) on the nanofluid molecules and thus reduces the velocity. Reducing the velocity of molecules adjacent to the wall weakens the boundary layer thickness growth and therefore increases the temperature gradient as well as the velocity gradient. The same is true for the trapezoidal-wall microchannel. Moreover, the MF greatly weakens the vortices and this results in a smaller thermal boundary thickness; as a result, heat transfer is improved.

Figure 7 illustrates how Nu_x changes for the base and trapezoidal-wall microchannels. Clearly, in the no-slip condition ($\beta^* = 0$), the nanofluid velocity at the microchannel wall is zero, which implies that it is stuck to the wall. By applying a slip condition, the molecules

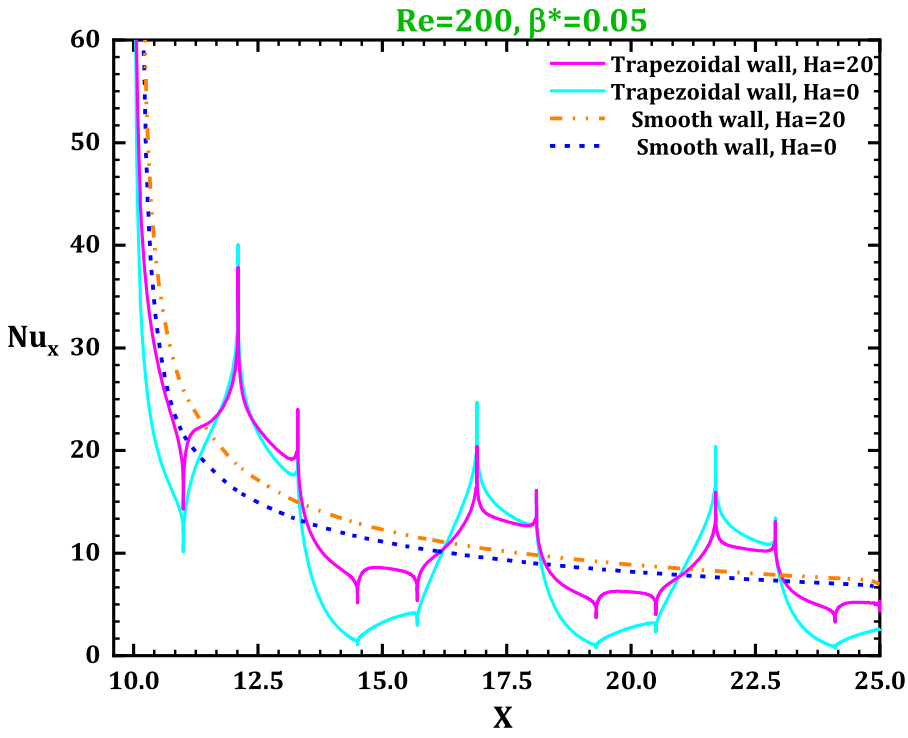

Figure 6. Variations in Nu_x for base and trapezoidal-wall microchannels in two scenarios (without/with an MF).

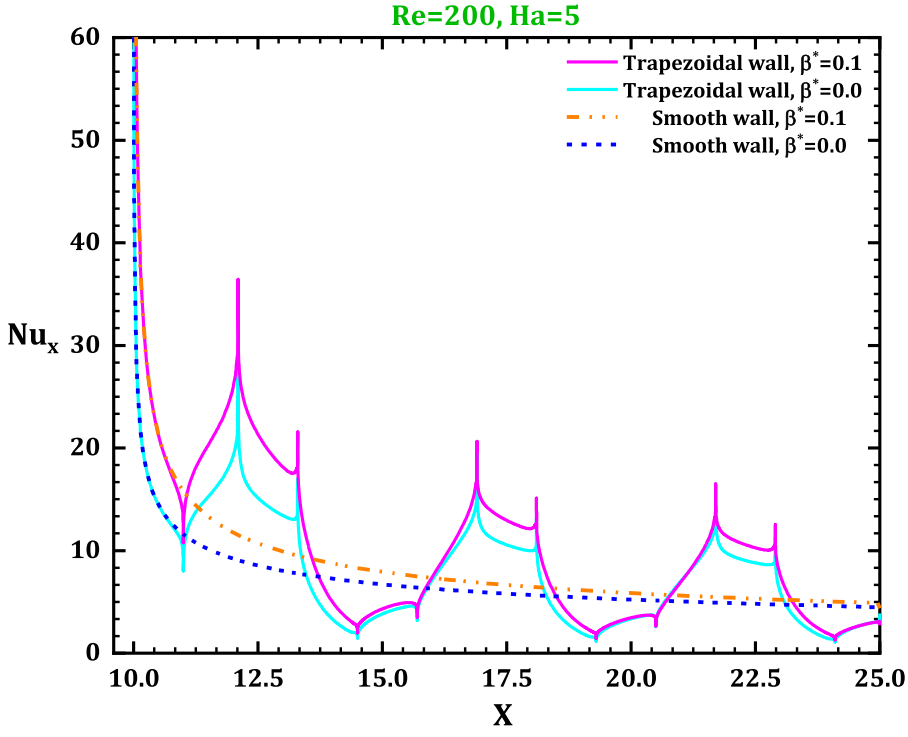

Figure 7. Variations in Nu_x for base and trapezoidal-wall microchannels at $\beta^* = 0$ (no-slip) and $\beta^* = 0.1$ (slip condition).

that are in direct contact with the wall do not stick and, by increasing the slip coefficient, the nanofluid molecules are replaced by other molecules at a lower temperature, thus increasing heat transfer.

The average Nusselt number variation (Figure 8) is illustrated at different Re, Ha and β^*. The sensitivity of the Nusselt number to Re, Ha and β^* is such that, as they increase, an improvement in the Nusselt number is

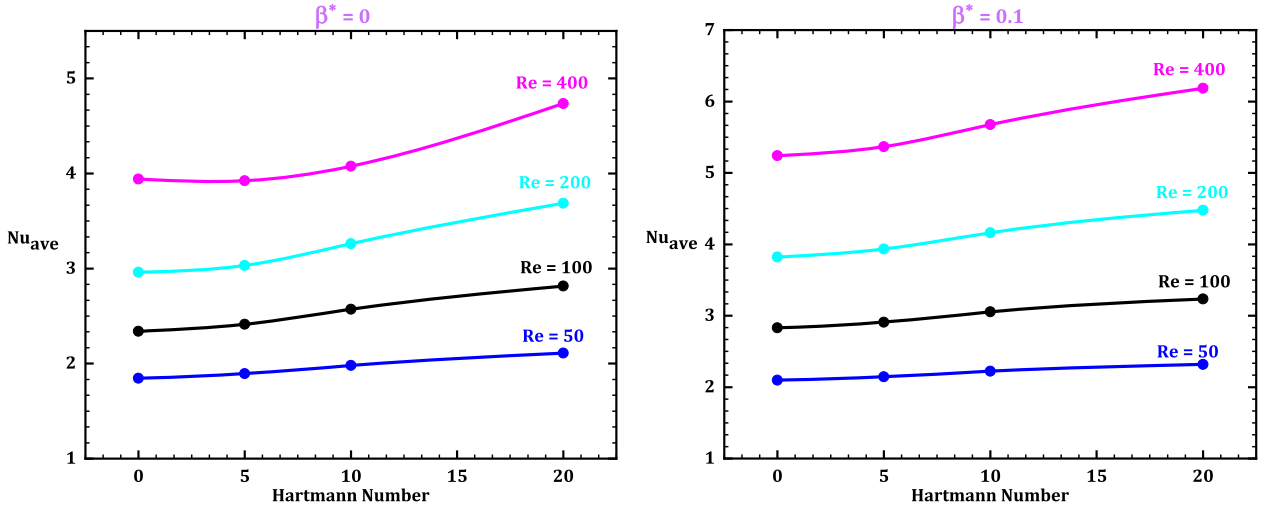

Figure 8. Variations in Nu_{ave} with respect to Ha at various Re and β^* values.

observed. As Re or Ha rises, the boundary layer thickness is reduced, hence temperature gradients, as well as heat transfer, are improved. The effect of an MF on improving heat transfer is affected by Re. The main purpose of using an MF in this study is to reduce the vortex strength. With an increase in Re, the possibility of vortex formation is reinforced. Thereby the effect of an MF in destroying them becomes more pronounced. For $\beta^* = 0.1$, at Re = 50, if the magnetic intensity (Ha) is boosted from 0 to 20, the average Nusselt number is intensified by 10.4%, while at Re = 400, it is amplified by 18%. Note that at $\beta^* = 0$, these figures are 14.31% (for Re = 50) and 20.13% (for Re = 400), respectively.

It should be noted that, in the presence of slip velocity, the vortex formation probability is less and therefore the effect of an MF on diminishing the vortex intensity becomes less and less. In conclusion, it can be said that, at higher Re and in the non-slip condition, the possibility of vortex formation is more, and in this case, the use of an MF has more obvious positive effects.

5.3. Comparison of heat transfer in trapezoidal-wall and base microchannels

In this section, heat transfer in the trapezoidal-wall is compared with that the base case. As shown in Figure 9, for all Re and Ha (with slip/non-slip conditions) the value of $Nu_{trapezoidal-wall}/Nu_{base}$ is greater than one, which means that heat transfer from the microchannel with trapezoidal-walls is higher than the corresponding value in the base microchannel. The effect of creating trapezoidal ribs on heat transfer is influenced by the values of Re, Ha and β^*. Since the problem with trapezoidal-walls is creating vortices, any factor that reduces the vortex formation probability leads to better performance.

Therefore, the following conclusions can be drawn.

1. With increasing Re number, the probability of vortex formation increases. Therefore, with increasing Re, the positive effect of using trapezoidal-walls diminishes. This is because, at high Re, the heat transfer capability is low in the vortex region. As shown in Figure 9, the value of Nu/Nu_{base} is reduced by increasing Re.
2. With increasing β^*, the probability of vortex formation reduces and therefore it is expected that the effect of trapezoidal-walls on heat transfer is greater. As shown in Figure 9, the value of Nu/Nu_{base} is raised by increasing β^*.
3. With increasing Ha, the vortex disappears and therefore the positive effect of increasing the heat transfer area (owing to using trapezoidal ribs) is more pronounced. As shown in Figure 9, the value of Nu/Nu_{base} is amplified by increasing Ha.

5.4. Entropy generation

In this section, entropy generation through a trapezoidal-wall microchannel is discussed. According to Equations (12) and (13), it can be observed that the values of gradients (of temperature/velocity) have a significant effect on entropy generation. On the other hand, the temperature gradient near the heating source and the velocity gradient near the wall have the highest values. Therefore, it is expected that the highest viscous entropy generation occurs near the wall and the highest thermal entropy generation is near the heating source. This trend is shown in Figures 10 and 11 for thermal entropy generation and Figures 12 and 13 for viscous entropy generation.

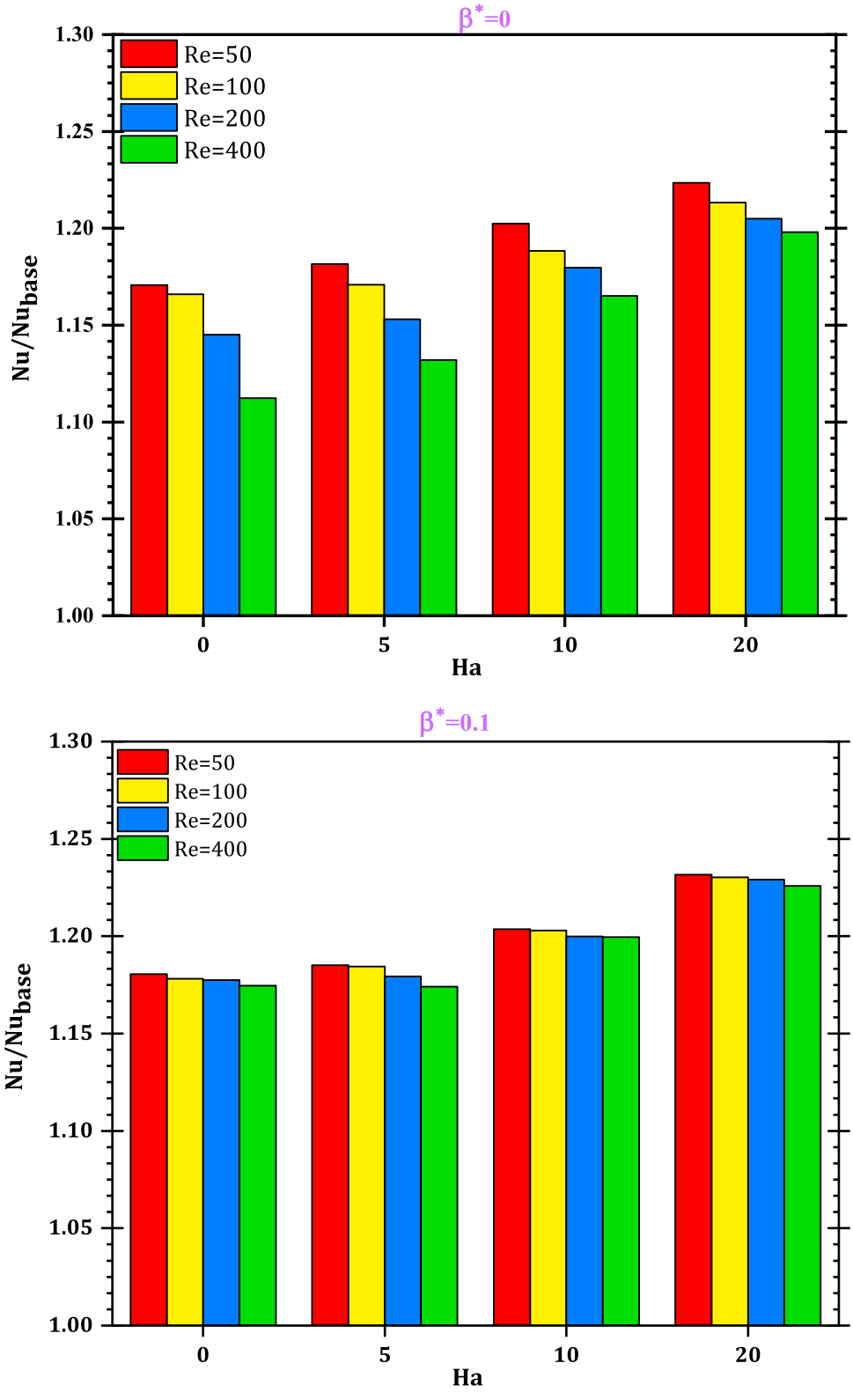

Figure 9. Trapezoidal rib microchannel heat transfer compared to base microchannel.

Figure 10 shows that, as Ha rises, $\dot{S}_{th}$ increases owing to temperature gradient growth (see Figure 5). Therefore, it should be noted that an MF enhances heat transfer irreversibly. In other words, the increase in heat transfer due to exerting an MF is accompanied by irreversibility.

The values of thermal entropy generation as well as viscous entropy generation are reported in Table 3, the

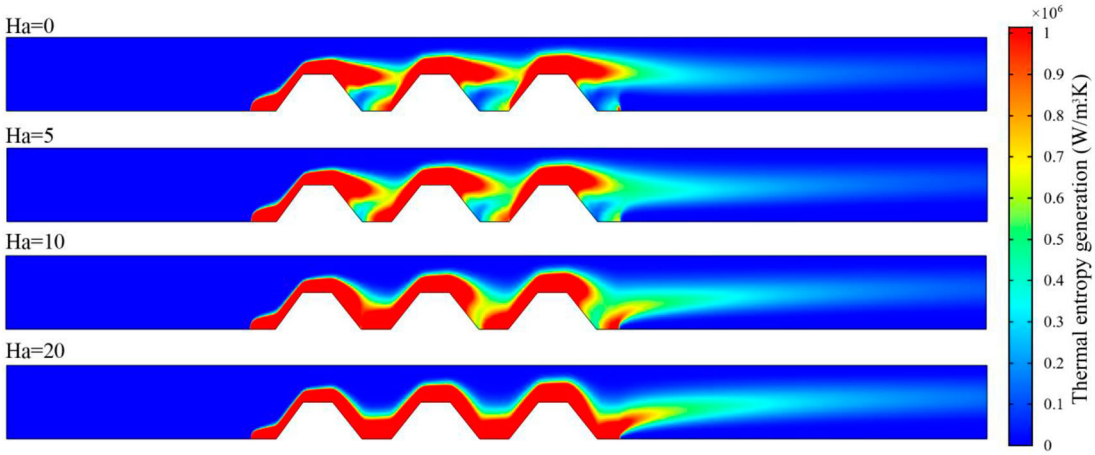

Figure 10. Distribution of thermal entropy generation for various *Ha*.

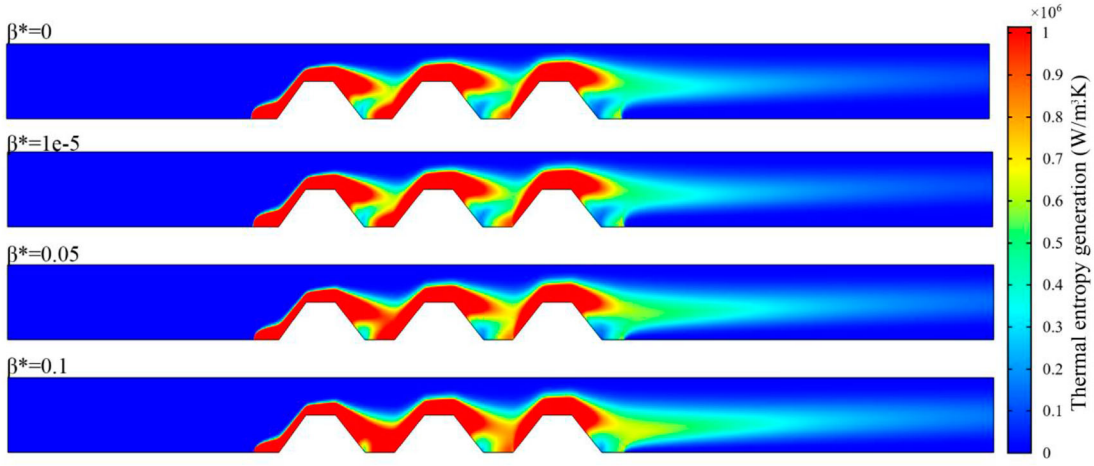

Figure 11. Distribution of thermal entropy generation for various β^*.

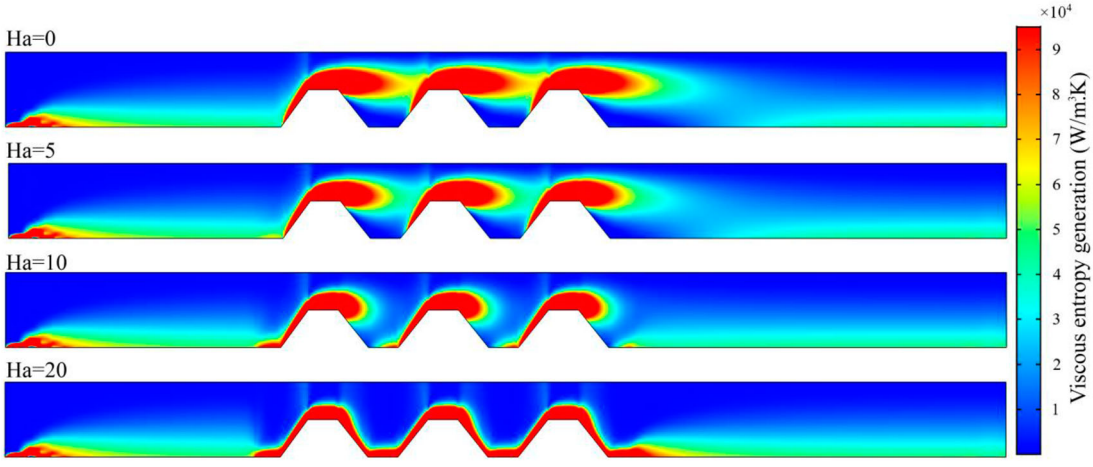

Figure 12. Distribution of viscous entropy generation for various *Ha*.

most important results of which are summarized as follows.

1. The amount of thermal entropy generation is much higher than viscous entropy generation, which means that the total entropy generation variation is similar to the thermal one.
2. It has already been mentioned that the effects of an MF on heat transfer is influenced by Re and β^*. In general, the use of an MF in conditions with a high

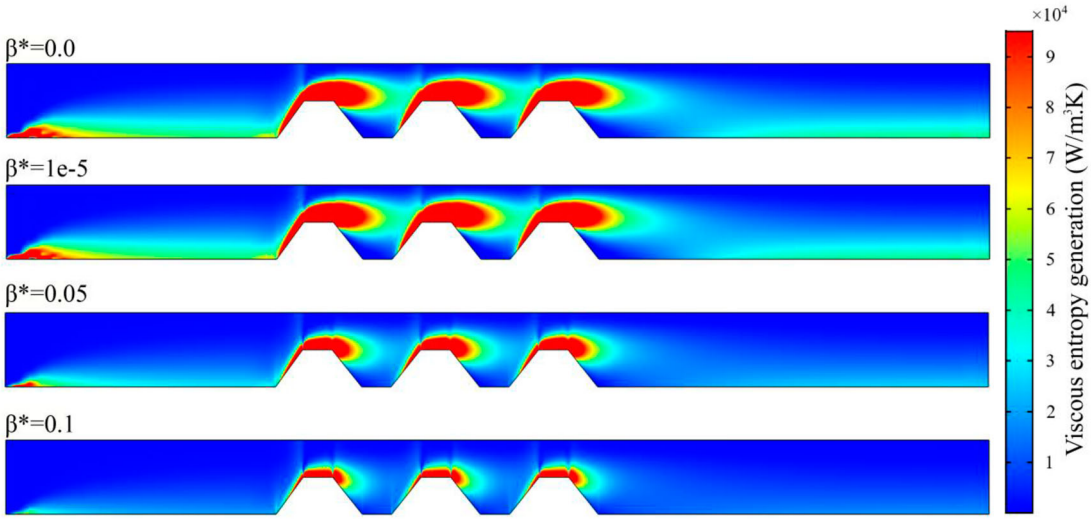

Figure 13. Distribution of viscous entropy generation for various β^*.

Table 3. Values of entropy generation (thermal/viscous).

		Entropy generation (W/m.K)							
		Friction				Thermal			
		Re = 50	Re = 100	Re = 200	Re = 400	Re = 50	Re = 100	Re = 200	Re = 400
$\beta^* = 0$	0	0.00042	0.001797	0.007923	0.036377	0.067948	0.094824	0.12464	0.16682
	5	0.000418	0.001758	0.007654	0.034949	0.069135	0.097198	0.12701	0.16583
	10	0.000435	0.001787	0.00754	0.033271	0.071303	0.10223	0.13486	0.17075
	20	0.00053	0.002144	0.008777	0.031788	0.074396	0.10984	0.1495	0.19404
$\beta^* = 10^{-6}$	0	0.00042	0.001797	0.007921	0.036366	0.067949	0.094828	0.12464	0.16583
	5	0.000418	0.001757	0.007652	0.034938	0.069137	0.097201	0.12702	0.16684
	10	0.000435	0.001787	0.007537	0.033259	0.071305	0.10223	0.13487	0.17077
	20	0.00053	0.002143	0.008773	0.031771	0.074397	0.10984	0.1495	0.19405
$\beta^* = 0.05$	0	0.000199	0.000834	0.003583	0.015803	0.072063	0.10522	0.14467	0.19727
	5	0.000187	0.000768	0.003248	0.014253	0.073261	0.1077	0.14798	0.19979
	10	0.000173	0.000695	0.002829	0.011888	0.075295	0.11255	0.15597	0.20943
	20	0.00016	0.000641	0.002566	0.010291	0.077812	0.11903	0.16862	0.23025
$\beta^* = 0.1$	0	0.000124	0.000519	0.002213	0.009543	0.074039	0.10998	0.15322	0.20975
	5	0.000114	0.000467	0.001959	0.008414	0.075125	0.11233	0.15669	0.21371
	10	0.000101	0.000407	0.001644	0.006792	0.076851	0.11654	0.16391	0.22361
	20	9.05E-05	0.00036	0.001425	0.005612	0.078793	0.12164	0.17397	0.2404

probability of vortex formation has more obvious positive effects. On the other hand, at high Re and low β^*, a vortex is more likely to form. In this case, the use of an MF has more effect (see Section 5.2). Therefore, it can be claimed that, in this condition (high Re and low slip coefficient), the effect of an MF on thermal entropy generation is also greater. At $\beta^* = 0$ and Re = 400 (where vortex formation probability is high(, an increment in Ha from 0 to 20 amplifies thermal entropy generation by 16.31%. It is expected that, with decreasing Re and increasing β^* (reducing the vortex formation probability), MF efficacy on thermal entropy generation will decrease. The computation reveals that this figure for $\beta^* = 0.1$ and Re = 50 is 6.42%.

3. In the previous section, it was observed that the maximum value of the mean Nusselt number occurs when the temperature gradient reaches its maximum value. All three parameters, Re, Ha and β^*, affect the temperature gradient. Growths in Re, Ha and β^* intensify the temperature gradient and thus increase entropy production. The results show that the highest thermal entropy generation (0.246 $\frac{W}{m.k}$) occurs at the highest values of Re, Ha and β^* (400, 20 and 0.1).

6. Conclusions

In this study, heat transfer in a simple microchannel (the 'base' case) and a microchannel with trapezoidal-walls is investigated. At the micro dimension, the slip condition affects the growth of the boundary layer. As such, slip coefficient efficacy on heat transfer is examined. In addition, the effects of MF application on heat transfer and entropy generation are evaluated. The most important results are as follows.

- The performance of a microchannel with trapezoidal walls is highly dependent on vortex formation. The

results show that, with vortex formation, heat transfer is reduced.

- With increasing Re number, the possibility of vortex formation in microchannels with trapezoidal-walls is intensified. Therefore, with increasing Re, although heat transfer rises, the effect of the presence of a trapezoidal-wall on heat transfer improvement is lost. At $\beta^* = 0$ and Ha $= 0$, if trapezoidal ribs are installed to a simple microchannel, heat transfer increases by 17% at Re $= 50$ and 11.2% at Re $= 400$. This is because, at higher Re, using ribs may lead to vortex formation, which decreases heat transfer.
- As the slip coefficient is increased, the effects of adding trapezoidal ribs on heat transfer are augmented. At $\beta^* = 0$, owing to adding ribs, heat transfer can be augmented up to 22.3%. At $\beta^* = 0.1$, this figure is 23.16%.
- The presence of an MF destroys vortices. Therefore, it is expected that, in the presence of an MF, the addition of ribs will have a greater effect on heat transfer. At $\beta^* = 0$ and Re $= 50$, adding ribs enhances heat transfer by 11.2% at Ha $= 0$ and 20% at Ha $= 20$, respectively.
- Computations show that the use of trapezoidal ribs in all conditions has a positive effect on heat transfer. The greatest effect of using ribs is a 23.16% increase in heat transfer, which occurs at the lowest Re and highest Ha and slip coefficient.
- Heat transfer and entropy generation in a microchannel with trapezoidal ribs is intensified with increasing slip coefficient, Ha and Re.

Nomenclature

a	Trapezius short length (μm)
b	Trapezius long length (μm)
B_o	Magnetic field strength (T)
C_p	Specific heat (J/kg · K)
E	Electric field
F	Lorentz force
h	Microchannel height (μm)
H	Dimensionless microchannel height
Ha	Hartmann number
l	Microchannel length (μm)
J	Current density (A/m^2)
L	Dimensionless microchannel
MF	Magnetic field
Nu	Nusselt number
Pr	Prandtl number
$\bar{p}$	Pressure (Pa)
P	Dimensionless pressure
$\ddot{q}$	Heat flux (W/m^2)
Re	Reynolds number
$\dot{S}_f$	Frictional entropy generation (W/m^3 · K)
$\dot{S}_{th}$	Thermal entropy generation (W/m^3 · K)
T	Temperature (K)
u	Horizontal velocity (m/s)
U	Dimensionless horizontal velocity
u_s	Slip velocity (m/s)
U_s	Dimensionless slip velocity
v	Vertical velocity (m/s)
V	Dimensionless vertical velocity
x	Horizontal axis
X	Dimensionless horizontal axis
y	Vertical axis
Y	Dimensionless vertical axis

Greek symbols

β	Slip coefficient (μm)
β^*	Dimensionless slip coefficient
φ	Volume fraction of nanoparticles (%)
μ	Dynamic viscosity (N · s/m^2)
τ	Shear stress (Pa)
θ	Dimensionless temperature
ρ	Density (kg/m^3)
υ	Kinematic viscosity (m^2/s)
α	Thermal diffusivity m^2/s
σ	Electrical conductivity (S/cm)

Super and subscripts

ave	average
c	cold
f	fluid
h	hot
nf	nanofluid
s	solid
th	thermal

Acknowledgements

The open access funding is by the publication fund of the TU Dresden.

Disclosure statement

No potential conflict of interest was reported by the authors.

ORCID

Dariush Bahrami http://orcid.org/0000-0001-6676-4458
Kwok-Wing Chau http://orcid.org/0000-0001-6457-161X
Amir Mosavi http://orcid.org/0000-0003-4842-0613

References

Abdollahi, A., Norris, S. E., & Sharma, R. N. (2020). Fluid flow and heat transfer of liquid-liquid Taylor flow in square microchannels. *Applied Thermal Engineering*, *115123*(5), 122–133. https://doi.org/10.1016/j.applthermaleng.2020.115123

Afrand, M., Karimipour, A., Nadooshan, A. A., & Akbari, M. (2016). The variations of heat transfer and slip velocity of FMWNT-water nano-fluid along the micro-channel in the lack and presence of a magnetic field. *Physica E: Low-Dimensional Systems and Nanostructures*, *84*, 474–481. https://doi.org/10.1016/j.physe.2016.07.013

Akermann, K., Renze, P., Dietl, J., & Schröder, W. (2020). Large-Eddy simulation of turbulent heat transfer in a multiple-started helically rib-roughened pipe. *International Journal of Heat and Mass Transfer*, *154*, 119667. https://doi.org/10.1016/j.ijheatmasstransfer.2020.119667

Alfellag, M. A., Ahmed, H. E., & Kherbeet, A. S. (2020). Numerical simulation of hydrothermal performance of minichannel heat sink using inclined slotted plate-fins and triangular pins. *Applied Thermal Engineering*, *164*, 114509. https://doi.org/10.1016/j.applthermaleng.2019.114509

Alipour, A., Korayem, M., & Younesian, D. (2019). Design and simulation of a magnetohydrodynamic micro-pump to provide time varying tensile force for vibration suppression in viscoelastic micro-beams. *Journal of Mechanical Science and Technology*, *33*(5), 2149–2159. https://doi.org/10.1007/s12206-019-0417-8

Amrollahi, A., Rashidi, A., Lotfi, R., Meibodi, M. E., & Kashefi, K. (2010). Convection heat transfer of functionalized MWNT in aqueous fluids in laminar and turbulent flow at the entrance region. *International Communications in Heat and Mass Transfer*, *37*(6), 717–723. https://doi.org/10.1016/j.icheatmasstransfer.2010.03.003

Arjmandfard, A., Toghraie, D., Mehmandoust, B., Hashemian, M., & Karimipour, A. (2020). The study of atomic porosity effect on water/Fe nanofluid flow in a microchannel with a molecular dynamics method. *Journal of Molecular Liquids*, *317*, 114291. https://doi.org/10.1016/j.molliq.2020.114291

Bahrami, D., Abbasian-Naghneh, S., Karimipour, A., & Karimipour, A. (2020). Efficacy of injectable rib height on the heat transfer and entropy generation in the microchannel by affecting slip flow. *Mathematical Methods in the Applied Sciences*, 312–344. https://doi.org/10.1002/mma.6728

Bahrami, D., Nadooshan, A. A., & Bayareh, M. (2020). Numerical study on the effect of planar normal and Halbach magnet arrays on micromixing. *International Journal of Chemical Reactor Engineering*, *1*(ahead-of-print).

Bayareh, M. (2020). An updated review on particle separation in passive microfluidic devices. *Chemical Engineering and Processing-Process Intensification*, *107984*, 66–76. https://doi.org/10.1016/j.cep.2020.107984.

Bayareh, M., Esfahany, M. N., Afshar, N., & Bastegani, M. (2020). Numerical study of slug flow heat transfer in microchannels. *International Journal of Thermal Sciences*, *147*, 106118. https://doi.org/10.1016/j.ijthermalsci.2019.106118

Cheng, L., Zhu, Y., Band, S. S., Bahrami, D., Kalbasi, R., Karimipour, A., … Mosavi, A. (2021). Role of gradients and vortexes on suitable location of discrete heat sources on a sinusoidal-wall microchannel. *Engineering Applications of Computational Fluid Mechanics*, *15*(1), 1176–1190. https://doi.org/10.1080/19942060.2021.1953608

Dehkordi, K. G., Karimipour, A., Afrand, M., Toghraie, D., & Isfahani, A. H. M. (2021). Molecular dynamics simulation concerning nanofluid boiling phenomenon affected by the external electric field: Effects of number of nanoparticles through Pt, Fe, and Au microchannels. *Journal of Molecular Liquids*, *324*, 114775. https://doi.org/10.1016/j.molliq.2020.114775

Dehkordi, R. B., Toghraie, D., Hashemian, M., Aghadavoudi, F., & Akbari, M. (2021). The effects of external force and electrical field on the agglomeration of Fe3O4 nanoparticles in electroosmotic flows in microchannels using molecular dynamics simulation. *International Communications in Heat and Mass Transfer*, *122*, 105182. https://doi.org/10.1016/j.icheatmasstransfer.2021.105182

Dinarvand, M., Abolhasani, M., Hormozi, F., & Bahrami, Z. (2021). Cooling capacity of magnetic nanofluid in presence of magnetic field based on first and second laws of thermodynamics analysis. *Energy Sources, Part A: Recovery, Utilization, and Environmental Effects*, 1–17. https://doi.org/10.1080/15567036.2021.1872746

Dinarvand, M., Sohrabi, M., Royaee, S. J., & Zeynali, V. (2017). Degradation of phenol by heterogeneous Fenton process in an impinging streams reactor with catalyst bed. *Asia-Pacific Journal of Chemical Engineering*, *12*(4), 631–639. https://doi.org/10.1002/apj.2104

Forghani-Tehrani, P., Karimipour, A., Afrand, M., & Mousavi, S. (2017). Different nano-particles volume fraction and Hartmann number effects on flow and heat transfer of water-silver nanofluid under the variable heat flux. *Physica E: Low-Dimensional Systems and Nanostructures*, *85*, 271–279. https://doi.org/10.1016/j.physe.2016.07.016

Gallegos, R. K. B., & Sharma, R. N. (2017). Flags as vortex generators for heat transfer enhancement: Gaps and challenges. *Renewable and Sustainable Energy Reviews*, *76*, 950–962. https://doi.org/10.1016/j.rser.2017.03.115

Gravndyan, Q., Akbari, O. A., Toghraie, D., Marzban, A., Mashayekhi, R., Karimi, R., & Pourfattah, F. (2017). The effect of aspect ratios of rib on the heat transfer and laminar water/TiO2 nanofluid flow in a two-dimensional rectangular microchannel. *Journal of Molecular Liquids*, *236*, 254–265. https://doi.org/10.1016/j.molliq.2017.04.030

Jiang, G., Gao, J., Shi, X., Li, F., & Xu, L. (2020). Flow and heat transfer characteristics of the mist/steam two-phase flow cooling the rectangular channel with column-row-ribs. *International Journal of Heat and Mass Transfer*, *156*, 119737. https://doi.org/10.1016/j.ijheatmasstransfer.2020.119737

Kalbasi, R. (2021). Introducing a novel heat sink comprising PCM and air – Adapted to electronic device thermal management. *International Journal of Heat and Mass Transfer*, *169*, 120914. https://doi.org/10.1016/j.ijheatmasstransfer.2021.120914

Karimipour, A., Bahrami, D., Kalbasi, R., & Marjani, A. (2020). Diminishing vortex intensity and improving heat transfer by applying magnetic field on an injectable slip microchannel containing FMWNT/water nanofluid. *Journal of Thermal Analysis and Calorimetry*, *77*, 1–12. https://doi.org/10.1007/s10973-020-10261-5

Karimipour, A., D'Orazio, A., & Shadloo, M. S. (2017). The effects of different nano particles of Al2O3 and Ag on the MHD Nano fluid flow and heat transfer in a microchannel including slip velocity and temperature jump. *Physica E:*

Low-Dimensional Systems and Nanostructures, *86*, 146–153. https://doi.org/10.1016/j.physe.2016.10.015

Mohebbi, R., Rashidi, M., Izadi, M., Sidik, N. A. C., & Xian, H. W. (2018). Forced convection of nanofluids in an extended surfaces channel using lattice Boltzmann method. *International Journal of Heat and Mass Transfer*, *117*, 1291–1303. https://doi.org/10.1016/j.ijheatmasstransfer.2017.10.063

Muhammad, A., Selvakumar, D., & Wu, J. (2020). Numerical investigation of laminar flow and heat transfer in a liquid metal cooled mini-channel heat sink. *International Journal of Heat and Mass Transfer*, *150*, 119265. https://doi.org/10.1016/j.ijheatmasstransfer.2019.119265

Nguyen, Q., Bahrami, D., Kalbasi, R., & Bach, Q. V. (2020). Nanofluid flow through microchannel with a triangular corrugated wall: Heat transfer enhancement against entropy generation intensification. *Mathematical Methods in the Applied Sciences*, *33*. https://doi.org/10.1002/mma.6705

Nguyen, Q., Bahrami, D., Kalbasi, R., & Karimipour, A. (2020). Functionalized multi-walled carbon Nano tubes nanoparticles dispersed in water through an magneto hydro dynamic nonsmooth duct equipped with sinusoidal-wavy wall: Diminishing vortex intensity via nonlinear Navier–Stokes equations. *Mathematical Methods in the Applied Sciences*.

Nojoomizadeh, M., & Karimipour, A. (2016). The effects of porosity and permeability on fluid flow and heat transfer of multi walled carbon nano-tubes suspended in oil (MWCNT/oil Nano-fluid) in a microchannel filled with a porous medium. *Physica E: Low-Dimensional Systems and Nanostructures*, *84*, 423–433. https://doi.org/10.1016/j.physe.2016.07.020

Ravi, B. V., Singh, P., & Ekkad, S. V. (2017). Numerical investigation of turbulent flow and heat transfer in two-pass ribbed channels. *International Journal of Thermal Sciences*, *112*, 31–43. https://doi.org/10.1016/j.ijthermalsci.2016.09.034

Salman, S. D. (2019). Comparative study on heat transfer enhancement of nanofluids flow in ribs tube using CFD simulation. *Heat Transfer-Asian Research*, *48*(1), 148–163. https://doi.org/10.1002/htj.21376

Samadifar, M., & Toghraie, D. (2018). Numerical simulation of heat transfer enhancement in a plate-fin heat exchanger using a new type of vortex generators. *Applied Thermal Engineering*, *133*, 671–681. https://doi.org/10.1016/j.applthermaleng.2018.01.062

Sheikholeslami, M., & Rokni, H. B. (2017). Simulation of nanofluid heat transfer in presence of magnetic field: A review. *International Journal of Heat and Mass Transfer*, *115*, 1203–1233. https://doi.org/10.1016/j.ijheatmasstransfer.2017.08.108

Shen, B., Yan, H., Sunden, B., Xue, H., & Xie, G. (2017). Forced convection and heat transfer of water-cooled microchannel heat sinks with various structured metal foams. *International Journal of Heat and Mass Transfer*, *113*, 1043–1053. https://doi.org/10.1016/j.ijheatmasstransfer.2017.06.004

Shiriny, A., Bayareh, M., Nadooshan, A. A., & Bahrami, D. (2019). Forced convection heat transfer of water/FMWCNT nanofluid in a microchannel with triangular ribs. *SN Applied Sciences*, *1*(12), 1631. https://doi.org/10.1007/s42452-019-1678-7

Turkyilmazoglu, M. (2011). Thermal radiation effects on the time-dependent MHD permeable flow having variable viscosity. *International Journal of Thermal Sciences*, *50*(1), 88–96. https://doi.org/10.1016/j.ijthermalsci.2010.08.016

Turkyilmazoglu, M. (2016). Natural convective flow of nanofluids past a radiative and impulsive vertical plate. *Journal of Aerospace Engineering*, *29*(6), 04016049. https://doi.org/10.1061/(ASCE)AS.1943-5525.0000643

Turkyilmazoglu, M. (2020a). Magnetohydrodynamic liquid plug running in a micro-channel: Analytical solutions. *Journal of Biomechanical Engineering*, *33*, 155–277. https://doi.org/10.1115/1.4048713

Turkyilmazoglu, M. (2020b). Nanoliquid film flow due to a moving substrate and heat transfer. *The European Physical Journal Plus*, *135*(10), 1–13. https://doi.org/10.1140/epjp/s13360-020-00812-y

Turkyilmazoglu, M. (2020c). Single phase nanofluids in fluid mechanics and their hydrodynamic linear stability analysis. *Computer Methods and Programs in Biomedicine*, *187*, 105171. https://doi.org/10.1016/j.cmpb.2019.105171

Turkyilmazoglu, M. (2021). On the transparent effects of Buongiorno nanofluid model on heat and mass transfer. *The European Physical Journal Plus*, *136*(4), 1–15. https://doi.org/10.1140/epjp/s13360-021-01359-2

Wang, G., Niu, D., Xie, F., Wang, Y., Zhao, X., & Ding, G. (2015). Experimental and numerical investigation of a microchannel heat sink (MCHS) with micro-scale ribs and grooves for chip cooling. *Applied Thermal Engineering*, *85*, 61–70. https://doi.org/10.1016/j.applthermaleng.2015.04.009

Wang, G., Qian, N., & Ding, G. (2019). Heat transfer enhancement in microchannel heat sink with bidirectional rib. *International Journal of Heat and Mass Transfer*, *136*, 597–609. https://doi.org/10.1016/j.ijheatmasstransfer.2019.02.018

Xu, Z., Lu, Y., Wang, B., Zhao, L., Chen, C., & Xiao, Y. (2019). Experimental evaluation of 100kW grade micro humid air turbine cycles converted from a microturbine. *Energy*, *175*, 687–693. https://doi.org/10.1016/j.energy.2019.03.036

Zhong, J.-F., Sedeh, S. N., Lv, Y.-P., Arzani, B., & Toghraie, D. (2021). Investigation of Ferro-nanofluid flow within a porous ribbed microchannel heat sink using single-phase and two-phase approaches in the presence of constant magnetic field. *Powder Technology*, *387*, 251–260. https://doi.org/10.1016/j.powtec.2021.04.033